

1 **Graphitic carbon nitride based (g-C₃N₄) nanocomposites for the**
2 **photodegradation of organic pollutants under visible light**
3 **irradiation: progress and future perspectives**

4
5 Bentuo Xu^{ab}, Mohammad Boshir Ahmed^a, John L. Zhou^{*a}, Ali Altaee^a, Gang Xu^b, Minghong
6 Wu^b

7
8
9
10 ^aSchool of Civil and Environmental Engineering, University of Technology Sydney, 15
11 Broadway, NSW 2007, Australia

12
13
14 ^bSchool of Environmental and Chemical Engineering, Shanghai University, Shanghai 200444,
15 China

16
17
18 Corresponding author:

19 Prof John L. Zhou

20 School of Civil and Environmental Engineering

21 University of Technology Sydney

22 15 Broadway, NSW 2007

23 Australia

24 Email:

junliang.zhou@uts.edu.au

25

26 **Abstract**

27 Graphitic carbon nitride (g-C₃N₄) has drawn great attention recently because of its visible
28 light response, suitable band gap, good redox ability, and metal-free nature. Compared with
29 common catalyst of TiO₂, g-C₃N₄ owns better photocatalytic ability and more energy-
30 efficient process as visible light could be directly utilized in g-C₃N₄ catalysis system.
31 Nevertheless, pure g-C₃N₄ still suffers the drawbacks of insufficient light adsorption, small
32 surface area and fast recombination of photogenerated electron and hole pairs. This review
33 summarizes the recent progress in the development of g-C₃N₄ composites to degrade
34 environmental organic pollutants in water. Element doping has been reported to be an
35 efficient method to promote the degradation efficacy and K doping was proven to be better
36 than other metal elements doping. In addition, semiconductor doping usually has a better
37 degradation performance as in the degradation of Ag₃PO₄-g-C₃N₄ which took only 5 min for
38 the complete degrading 10 mg L⁻¹ of methyl orange (MO) under visible light irradiation and
39 the *k* is as high as 0.2357 min⁻¹. Moreover, doping with more than one compound defined as
40 co-doping has the ability to deal with more than one pollutant but still exhibited high rate
41 constant. When the stability is taken consideration, most of the g-C₃N₄ composites possess
42 high reusability and immobilization is regarded as a significant method to improve the
43 stability. Future studies should focus on the photocatalysis of persistent organic pollutants
44 (such as POPs) by the g-C₃N₄ in order to make a further evaluation for their catalytic ability
45 and the environmental conditions during the photocatalysis process that need to be provided
46 at the same time.

47

48 *Keywords:* Photocatalysis; g-C₃N₄ composites; Morphology; Co-doping; Immobilization

49

50
51
52
53
54
55
56
57
58
59
60
61
62
63
64
65
66
67
68
69
70
71

Contents

1. Introduction	4
2. Photocatalysis by g-C₃N₄	6
2.1. Photodegradation mechanism.....	6
2.2. Photodegradation ability.....	7
3. Modified g-C₃N₄ nanomaterials and their catalytic ability	8
3.1. Metal and non-metal doping.....	8
3.2. Semiconductor doping.....	12
3.3. Morphology controlling and co-doping.....	14
4. Stability of g-C₃N₄ nanocomposites	15
4.1. Reusability.....	16
4.2. Immobilization	17
5. Future perspectives	19
5.1. Photocatalysis of POPs.....	19
5.2. Influence of environmental conditions.....	20
6. Conclusions	21
Acknowledgements	22
References	24

72

73 1. Introduction

74 As the world is facing an increasing challenges in the fields of energy and
75 environmental pollution, the use of renewable energy to control of environmental pollution is
76 of high priority. As an inexhaustible and environmental friendly resource, solar energy is
77 considered to be the most ideal power and it makes the photolysis to be a favourable
78 technology for solving the environmental contamination [1, 2]. By comparison, other
79 treatment methods such as electrochemistry [3], filtration [4], biodegradation [5], and
80 membrane bioreactor [6] all have the **drawbacks** of consuming raw materials. However, for
81 the practical application of photolysis, low efficacy of solar energy utilization is the main
82 obstacle. Thus, photocatalysis, especially semiconductor photocatalysis, becomes popular due
83 to the advantages of using renewable resources, cost-effectiveness, safe, and comparatively
84 high removal efficacy of the pollutants [7]. For example, titanium dioxide (TiO₂) [8], zinc
85 oxide (ZnO) [9], bismuth sulfide (Bi₂S₃) [10], and carbon nitride (C₃N₄) [11] have been
86 reported **previous** to perform well in photocatalysis. These semiconductors possess the ability
87 to adsorb the light and produce photogenerated electron and hole pairs, which **have** redox
88 ability to degrade the environmental pollutants. In addition, doping of catalyst such as TiO₂
89 by Au has enabled the catalyst to perform significantly better under visible light [12].

90 Notably, C₃N₄ is a non-toxic, abundant and low cost material, and has a metal-free
91 property compared with other common catalysts [13]. In 1996, Teter and Hemley firstly
92 conducted research on the C₃N₄ material and provided five molecular structures: β-C₃N₄, α-
93 C₃N₄, g-C₃N₄, p-C₃N₄, and c-C₃N₄ (**Fig. S1**) [14]. Among them, g-C₃N₄ is most stable at
94 room temperature and atmosphere pressure with the lowest density. From the end of the
95 twentieth century, g-C₃N₄ has been extensively applied in many fields, including fuel cells,
96 photocatalysis, gas storage, reduction of carbon dioxide (CO₂), and splitting water to produce
97 hydrogen (H₂) [15-17]. As a catalyst, g-C₃N₄ has the moderate bandgap energy of 2.65 eV

98 which **ensures** it can utilize visible light directly in the 400-800 nm region [18, 19]. Moreover,
99 the redox ability of the transferred photoexcited carriers and excellent chemical stability
100 makes it potentially suitable for the solar energy conversion and pollutants adsorption.
101 Nevertheless, the pristine of g-C₃N₄ still suffers three main disadvantages including
102 insufficient absorption of light source, low surface area and the fast recombination of
103 photogenerated electron and hole pairs, leading to a comparatively low photodegradation
104 efficacy [20, 21]. Therefore, many routes have been developed to solve such problems and
105 promote the photocatalytic activity. For example, non-metal doping, metal doping, and
106 coupling with other semiconductors **are** known to be the **effectiveness methods**. The fusion of
107 two π -conjugated systems not only **enhances** the charge separation of electron and hole from
108 the single material, but also further increases the utilization region of solar spectra [19].
109 Moreover, morphology controlling is another effective method to promote the degradation
110 efficacy as it could significantly enlarge the surface area of the catalyst so that the adsorption
111 ability of light source and pollutants are both promoted [22].

112 The g-C₃N₄ and its modified composites have been successfully applied to the
113 remediation of organic pollutants. Basically, the colored dyes such as Rhodamine B (RhB),
114 methyl orange (MO), basic fuchsin (BF) and methylene blue (MB), were treated to evaluate
115 the catalytic ability of as-synthesized g-C₃N₄ composites [23-26]. Because dye pollutants are
116 not only now widely used in the textile, printing and plastic industries, but also hard to be
117 degraded in water due to their complex composition, deep color, and chemical and physical
118 stability. Dyes could absorb visible light irradiation and represent some of the principal
119 pollutants in the wastewater from the textile industry [27]. On the other hand, some other
120 organic compounds such as phenol, atrazine, and humic acid also have been reported to be
121 treated with g-C₃N₄ composites **under photocatalysis system**, which indicates that g-C₃N₄
122 owns the photocatalytic ability to deal with different kinds of environmental organic
123 pollutants in water [28-30].

124 There have been many publications on the application of g-C₃N₄ in water splitting, H₂
125 production, CO₂ reduction and photocatalysis [31-35]. In this review, we focused on the
126 evaluation of catalytic ability of g-C₃N₄ composites for the environmental organic pollutants
127 removal under visible light irradiation compared with common catalyst of TiO₂ nanoparticles,
128 and photodegradation mechanism. In addition, in order to further promote the degradation
129 efficacy, modifications on the g-C₃N₄ nanomaterials, including element or compound doping
130 and morphology controlling are discussed. Besides, the stability of these as-synthesized g-
131 C₃N₄ catalysts are introduced on the two sides of reusability and immobilization. In future
132 studies, the photocatalysis of different kinds of organic pollutants degraded by g-C₃N₄ is
133 highly recommended, and the effects of environmental conditions on photocatalysis process
134 should be fully investigated.

135

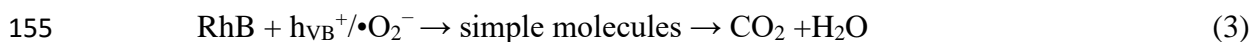
136 **2. Photocatalysis by g-C₃N₄**

137 Pure g-C₃N₄ has higher photocatalytic ability than TiO₂ when dealing with dye
138 pollutants and its photodegradation mechanism is related to the photoacted carriers
139 occurring in the photocatalysis system. the mechanisms and efficiency of g-C₃N₄ are
140 discussed below

141 **2.1. Photodegradation mechanism**

142 The photodegradation mechanism of organic pollutants over g-C₃N₄ is provided in
143 **Fig. S2A**. The band gap of g-C₃N₄ is 2.65 eV and **its** VB and CB potential is -1.09 and 1.56
144 eV, respectively [36]. So when g-C₃N₄ absorbs $h\nu$ with energy equal to or great than 2.65 eV,
145 the electron in CB will transfer to VB and in the meantime, a hole is generated in the CB. The
146 photogenerated electron and hole pair owns strong redox ability owing to the high VB
147 potential and low CB potential. **As a result**, the pollutants could be degraded directly by either
148 photogenerated electrons or the holes and the degradation efficacy largely depend on the
149 quantity of the electron-hole pairs and their redox ability. Besides, as the electrons is in a

150 comparatively low potential of -1.09 eV, they can react with the dissolved oxygen (DO) to
151 produce superoxide radicals ($\bullet\text{O}_2^-$), which also could be the active group to degrade
152 pollutants. Taking RhB as an example, the reaction process can be described as follows:



157 The photogenerated electron-hole pairs will soon be recombined so that their quantity
158 is reduced and largely limits the degradation efficacy [37]. Thus, inhibition of this
159 recombination would be a significant route to promote the efficacy. In addition, modifying the
160 band gap structure of the catalyst could broaden the range of light adsorption and thus
161 **improve** the quantity of electron-hole pairs. However, too narrow band gap will lead to the
162 low redox ability of the photogenerated electrons and holes even though they have high
163 quantity [38]. Thus, making the band gap to a suitable structure is the key point when
164 modifying the catalyst. And when the VB is improved to more than 1.99 eV, hole in the VB
165 potential can react with water to produce hydroxyl radicals ($\bullet\text{OH}$) scavenger as in Eq. 4,
166 which also has the ability to degrade pollutants in this system and further promotes the
167 degradation performance. Besides, controlling the morphology to a certain structure would
168 not only extend the specific surface area of $\text{g-C}_3\text{N}_4$ which is beneficial for the light
169 adsorption, but may also provide more active sites to contribute the photocatalysis. According
170 to these methods, many research studies have been performed and already got some
171 achievements in promoting degradation efficacy for the organic pollutants by **the modification**
172 **nanocomposites** of $\text{g-C}_3\text{N}_4$ materials [39-41].

173 2.2. Photodegradation ability

174 The photocatalytic activity of the pure $\text{g-C}_3\text{N}_4$ was investigated by some researchers
175 and 5 mg L^{-1} of RhB [42], 10 mg L^{-1} of MO [43], 3 mg L^{-1} of MB and 3.5 mg L^{-1} of BF [44]

176 were chose as the target pollutants to be degraded. The results are provided in **Fig. 1** which
177 indicates that these four organic pollutants all have shown 50% or more degradation within
178 120 min by pure g-C₃N₄ with visible light irradiation. This process could be considered as a
179 pseudo first-order reaction and its kinetics are calculated by the equation of $-\ln(C/C_0) = kt$,
180 where k (min⁻¹) is the degradation rate constant, C_0 and C (mg L⁻¹) are the absorption
181 equilibrium concentration of RhB and the concentration of the pollution at a reaction time of t
182 (min), respectively. According to this, the degradation efficacy of different pollutants follows
183 the order of $k_{RhB} = 0.0139 \text{ min}^{-1} > k_{MB} = 0.0074 \text{ min}^{-1} > k_{BF} = 0.0062 \text{ min}^{-1} > k_{MO} = 0.0041$
184 min^{-1} . This difference may be related to the various molecular composition and structure,
185 degree of charge, or adsorption quantity by the catalyst of these pollutants. For a comparison
186 purpose, 5 mg L⁻¹ of RhB [42], 5 mg L⁻¹ of MO [45], and 10 mg L⁻¹ of MB [46] were
187 conducted by TiO₂ nanoparticles photocatalysis as shown in **Fig. 1**. The results suggest that g-
188 C₃N₄ outperformed TiO₂ when dealing with these three pollutants especially RhB and MB, as
189 their k value of g-C₃N₄ is 4.2 and 3.4 times higher than that of TiO₂. Therefore, g-C₃N₄ is
190 proven to be a better catalyst than TiO₂ in degradation of organic pollutants. However,
191 according to the drawbacks mentioned in the photodegradation mechanism, it has much
192 potential to get stronger photocatalytic ability to degrade the environmental pollutants
193 efficiently.

194

195 **3. Modified g-C₃N₄ nanomaterials and their catalytic ability**

196 Based on the photodegradation mechanism, many novel g-C₃N₄ nanocomposites were
197 synthesized to overcome the drawbacks of the pristine and achieved comparatively high
198 degradation efficacy for the organic pollutants removal. The modification methods include
199 metal and non-metal doping, semiconductor doping, morphology controlling and co-doping.

200 **3.1. Metal and non-metal doping**

201 **Metal doping** can lower the band gap of the doped g-C₃N₄ composite and promote its
202 absorption of visible light, improve the specific surface area, and inhibit the recombination of
203 photogenerated electron-hole pairs. The reported metal-doped g-C₃N₄ catalysts are
204 summarized in **Table 1** with their characteristics and degradation efficacy [47-52]. **The results**
205 exhibit that europium (Eu) doped by Xu et al. [46] **has** the narrowest band gap **of 2.41 eV** and
206 tungsten (W) doped by Rong et al. [53] **extends** its surface area 5.5 times than the pristine
207 condition. However, the most effectiveness modification is **potassium** (K) doping as this
208 composite catalyst could promote the rate constant 6.5 times higher than the value of original
209 one [54]. Thus, it indicates that K is more suitable for enhancing the photocatalytic activity
210 than any other metals, which might be attributed to the following reasons: firstly, Obtaining
211 suitable band gap. Commonly, the lone pair electron of nitrogen has strong influence on the
212 electron density distribution [55], however, metal doping could change the electron density of
213 the N atoms, thus altering the electronic structure and band gap of carbon nitride as shown in
214 **Fig. 2A**. Notably, too high band gap energy will result in adequate quantity of photo-induced
215 electron-hole pairs produced in the catalytic system. On the opposite, too low band gap could
216 lead to the abundant electron-hole pairs but with weak oxidant-reduction ability. Therefore,
217 according to the results of the *k* value provided in **Table 1**, 2.57 eV is the most suitable band
218 gap for the catalyst of K doping. Secondly, K atoms tend to exist in the g-C₃N₄ interlayer via
219 bridging the layers rather than doping into the conjugated plane acting as Na atoms [35].
220 Meaningfully, such nanostructure can make K atoms chemically bond with atoms at the
221 adjacent two layers which benefit to forming charge delivery channels and bridging the
222 layers, contributing to the transfer and separation of electron-hole pairs (**Fig. S3**). Thirdly, as
223 the CB and VB potentials altered by K doping could be tuned from -1.09 to -0.53 eV and
224 from +1.56 to +2.04 eV, respectively, and hence •OH and •O₂⁻ could be formed, leading to
225 the improving efficacy of photodegradation (**Fig. 2A**). As a comparison, the CB and VB
226 potentials changed by W doping was -1.13 and +1.57 eV, which is not beneficial for the

227 production of $\bullet\text{OH}/\text{OH}^-$ (+1.99 eV). All in all, compared with pure g-C₃N₄, K doping
228 promoted most degrading efficacy of organic pollutants photodegradation than other metal
229 performance.

230 Although metal doping has many advantages in promoting the catalytic ability, the
231 drawbacks of poor thermal stability of the doped ions and losing metal-free property existed.
232 Thus, non-metal doping has been investigated on their high ionization energy and high electro
233 negative. As a result, no-metal doping could not only avoid the thermal variation of chemical
234 states of doped metal ions, but also keep the metal-free property of g-C₃N₄. **Table 1** provides
235 four kinds of non-metal doping and it shows that B doping promoted the efficacy 3.6 times
236 higher than the value of pure g-C₃N₄ and better than the performance of P, S and C doping
237 [56]. B doped with g-C₃N₄ were first synthesized by Yan et al. via heating the mixture of
238 melamine and boron oxide [57]. Ruan et al. calculated the forming energy of the doped
239 nanomaterial according to the Eq. 5 as follows [58]:

$$240 \quad E_{form} = E_{tot}(\text{X:C}_3\text{N}_4) - E_{tot} - \mu(\text{X}) + \mu(\text{C}) \quad (5)$$

241 where $E_{tot}(\text{X:C}_3\text{N}_4)$ is the total energy after element is doped; E_{tot} is the total energy before
242 element is doped; $\mu(\text{X})$ is the atomic energy of the doped element; $\mu(\text{C})$ is the atomic energy
243 of the alternative element. The results came out that the form energy of B, P and S doped
244 system were -1.76, 2.44 and 3.41 eV, respectively, which indicated that B was easy to be
245 doped in the carbon site as its energy value was negative while P and S were comparatively
246 hard to be doped as their doping process need adsorbing energy. Thus, B is easier to be doped
247 than P and S, which possibly explains the phenomenon that B doping performs best to
248 promote the degradation ability. Besides, recently a new doping method namely self-doping
249 has been investigated which can be defined as reintroducing the existed element of the
250 catalyst to change its nanostructure [59-61]. Dong et al. conducted C self-doping in CN
251 framework which could accelerate the electronic migration due to the formation of conjugate
252 big π bonds and stronger light absorption capacity [62]. As a result, the photo-induced

253 electron and hole pairs were increasing and their separation effect was better. In effect, C
254 doping promoted 3.0 times of rate constant for RhB degradation than **that of** origin g-C₃N₄.

255 Notably, the precursor of CN in the g-C₃N₄ composite catalyst has strong influence on
256 its photocatalytic ability for the organic pollutants removal. **Fig. S4** exhibits the photocatalytic
257 efficacy for RhB removal of g-C₃N₄ synthesized by different CN precursors. The results
258 indicate that urea as the precursor produced g-C₃N₄ with best degradation performance and
259 the order is: urea ($k=0.1973 \text{ min}^{-1}$) > melamine ($k=0.1890 \text{ min}^{-1}$) > cyanamide ($k=0.1863 \text{ min}^{-1}$)
260 > dicyandiamide ($k=0.1442 \text{ min}^{-1}$). During the urea reaction process, the step of thermal
261 polycondensation was much complex and many hetero atoms such as H and O were drawn off
262 as the form of small molecules. As a result, the C and N ratios in the products were relatively
263 high, which achieved high purity of g-C₃N₄ product. Therefore, g-C₃N₄ produced by urea has
264 well efficacy during the photocatalysis of RhB. However, its yield is as low as 8% and this
265 defect would lead to a large resource waste [63]. Thus, when both productive yield and
266 degradation efficacy are taken into consideration, melamine is preferable to be chosen as the
267 precursor. Similarly, the same element of metal or non-metal doped g-C₃N₄ from different
268 precursors possesses various morphology and photocatalytic ability as shown in **Table 1**. For
269 example, KOH and KI as precursors produced K-C₃N₄ catalysts with a different band gap of
270 2.57 and 2.64 eV, respectively [54, 64]. In addition, Fe-C₃N₄ prepared by FeCl₃ as precursor
271 had lower band gap of 2.56 and higher improved times efficacy of 5.8 than the one from
272 Fe(NO₃)₃•9H₂O precursor[42, 65]. Moreover, P doping synthesized by (NH₄)₂HPO₄, NH₄PF₆,
273 and BmimPF₆ also have various promoted efficacies [66-68]. Therefore, it may suggest that as
274 the same elements exist in different forms in different precursors, when they are doped in g-
275 C₃N₄ material, they need different extent of energy so that the synthetic effect and
276 morphology would be various. All in all, the precursors are significant factor related to the
277 synthetic catalyst and their photodegradation ability. So according to the data in **Table 1**, it is
278 reasonable to make a hypothesis **that K doping with** g-C₃N₄ synthesized by KOH and

279 melamine as the precursors will own the best catalytic ability than other materials shown in
280 table 1, but still needs to be proven by experiments in the future.

281 3.2. Semiconductor doping

282 When two semiconductors with different CB and VB potentials are doped together as
283 heterojunction, the photogenerated electrons and holes could transfer from the energy level of
284 one semiconductor to another's. From the **Table 2**, it proves that all the semiconductor doping
285 catalysts of g-C₃N₄ have the improving efficacy of organic pollutants degradation to varying
286 degrees when compared with the performance of pure g-C₃N₄ (k_p) and TiO₂ (k_T) [45, 53, 69-
287 76]. Particularly, CdS-g-C₃N₄ composites synthesized by Fu et al. could degrade MO (5 mg
288 L⁻¹) within 20 min and its k (0.00564 min⁻¹) was 11.2 and 14.0 times **higher than that** that of
289 the pristine and TiO₂, respectively [77]. Similarly, BiOBr-g-C₃N₄ prepared by Fu et al.
290 degraded 100% RhB (20 mg L⁻¹) within 40 min with the k of 0.0433 min⁻¹, which was almost
291 7.2 and 8.6 fold higher than that of the pristine and TiO₂ [78]. Degradation by BiOBr-g-C₃N₄
292 composites (**Fig. S2B**) is performed according to the following mechanism, the electrons
293 generated in the CB of g-C₃N₄ transfer to the CB of BiOBr and in the meantime, holes
294 generated in the VB of BiOBr transfer to the VB of g-C₃N₄. Thus, the photogenerated
295 electron and hole pairs are able to be separated effectively and promote the photodegradation
296 efficacy. Significantly, the band gap of the doped semiconductor is the key factor as it decides
297 the quantity of the transferred electrons and holes from one material to another and thus
298 indirectly influences the recombination rate of electron-hole pairs. As shown in **Fig. 2B**,
299 different semiconductors possess different VB and CB potentials and based on the results,
300 Ag₂O, BiOBr, CdS have comparatively more matched band gap structure in the composite
301 system than other compounds.

302 On the other hand, Z-Scheme composite doping is defined as **that** during the
303 photocatalytic procedure, the electrons generated in the CB of g-C₃N₄ transfer to VB of doped
304 compound rather than the same g-C₃N₄ and annihilate the holes in VB of the compound (two

305 different migration mechanisms of charges shown in **Fig. S2C and D**). Thus, it could inhibit
306 the electron-hole pairs recombination in both g-C₃N₄ and the doped compound. For example,
307 over Z-Scheme Ag₃PO₄-g-C₃N₄ hybrid photocatalysts, it took only 5 min for the complete
308 degradation of MO (10 mg L⁻¹) with visible light irradiation and the *k* is as high as 0.2357
309 min⁻¹ [79]. It may be contributed to the typical Z-scheme mechanism which is favourable for
310 organic pollutant degradation. Specifically, as shown in **Fig. 3D**, the electrons in CB of
311 Ag₃PO₄ migrate to the VB of g-C₃N₄ and combine with the holes there. So the recombination
312 rates of electron-hole in both g-C₃N₄ and Ag₃PO₄ are reduced. Thus, the electrons in CB of g-
313 C₃N₄ has strong reductive ability as its potential is as low as -1.15 eV so they can react with
314 DO to produce •O₂⁻ which is able to degrade MO. In the meantime, holes in the VB of
315 Ag₃PO₄ own strong oxidation ability because of its high potential (+2.69 eV) and the holes
316 can degrade MO directly. However, if the migration route of the charges follows the
317 conventional heterojunction electron-hole separation, the electrons in the CB of g-C₃N₄ would
318 transfer to the VB of Ag₃PO₄ and it can not produce •O₂⁻ with O₂ as the CB potential of
319 Ag₃PO₄ is more positive than that of O₂/•O₂⁻ couple. Moreover, the oxidation power of holes
320 in VB of g-C₃N₄ is decreasing due to the relatively low potentials (1.6 eV). Therefore,
321 theoretically, the Z-Scheme hybrid g-C₃N₄ composites perform better degradation capacity
322 than conventional heterojunction catalysts. According to the results summarized in **Table 2**,
323 when dealing with above 3 mg L⁻¹ of MB, Z-scheme WO₃-g-C₃N₄ could degrade almost MB
324 within 120 min with the *k* of 0.0353 min⁻¹ while only 90% MO were photodegraded within as
325 long as 300 min by TiO₂-g-C₃N₄ catalyst and its *k* is just 0.007 min⁻¹ [44]. In addition, Z-
326 Scheme Bi₂MoO₆ could degrade 90% of 10 mg L⁻¹ MO within 40 min and the *k* is 0.0688
327 min⁻¹ [80]. When dealing with 10 mg L⁻¹ of RhB, Z-Scheme SnO_{2-x} and Z-Scheme V₂O₅ both
328 could degrade almost of the pollutant within 60 min and their efficacies were better than that
329 of DyVO₄ and GdVO₄ [81-84]. Thus, based on the mechanism analysis and results
330 comparison, the Z-Scheme catalysts indeed have the better photodegradation ability but when

331 the cost of light energy and ambient conditions are taken into consideration, further researches
332 need to be done in the future.

333 3.3. Morphology controlling and co-doping

334 There is a close connection between the morphological structure of the catalyst and its
335 photocatalytic capacity. Many efforts have been paid on the morphology controlling and until
336 now, various types of the morphology worked out can be concluded as porous[85],
337 mesoporous [86], microspherical [87], and nanosheet g-C₃N₄ [88], etc. Done et al.
338 investigated the morphology controlling of tubular g-C₃N₄ and their visible light
339 photocatalytic properties [89]. The results are provided in **Table 3** and they exhibit that the
340 modified morphology, nanoflake, nanotube, and rod-like g-C₃N₄ all promoted the rate
341 constant to 0.0047, 0.0055, and 0.0058 min⁻¹, which were 1.3, 1.6, and 1.7 times higher than
342 that of the pristine. The Scanning Electron Microscope (SEM) images of the different
343 morphology structure catalyst are shown in **Fig. S5** and their better performance of
344 degradation can be attributed to the increased specific surface area which is suitable for
345 photocatalytic application. Thus, morphology controlling is **truly** an effective method of
346 modifying g-C₃N₄ to promote the photocatalytic ability. Besides, metal doping such as S and
347 Cu with morphology modification of porous rods and mesoporous, respectively both made the
348 catalysts own a better photocatalytic ability with the *k* values 12.8 and 4.3 times higher than
349 that of the pristine [43, 56].

350 Furthermore, co-doping is another significant method which could combine the
351 advantages of single material, leading to improved photocatalytic activity. Dual doping, such
352 as metal/non-metal doping or semiconductor doping both have been proved to have better
353 performance as discussed above. Recently, tridoping g-C₃N₄ is developed by combining three
354 different heteroatoms into g-C₃N₄ framework for modification. Moreover, with morphology
355 controlling, these tridoping g-C₃N₄ catalysts possess more benefits for the photodegradation
356 of organic pollutants (**Table 3**) [90, 91]. Notably, Ag@AgCl-g-C₃N₄ porous nanosheets

357 synthesized by Zhang et al. could degrade RhB, MB, MO, and Phenol as pollutants [92].
358 Especially, 10 mg L⁻¹ of RhB was completely degraded within 30 min with the *k* of 0.1954
359 min⁻¹ and 10 mg L⁻¹ of MB and MO both could be 100% degraded within 60 min. Even
360 though with comparatively lower rate constant, 10 mg L⁻¹ of Phenol still would be mostly
361 degraded (80%) within 140 min. Thus, this co-doping catalyst with morphology controlling
362 not only can degrade several kinds of dye pollutants, but also have high degradation efficacy
363 when dealing with different target pollutants. The major active species for the
364 photodegradation was identified as the holes and •O₂⁻. Besides, the holes could oxidize Cl⁻
365 ions from AgCl to •Cl, which is also able to degrade dye pollutants as the active radical
366 species. In addition, the synergistic interaction of Ag and polarization field around AgCl and
367 the matching band gap of AgCl and g-C₃N₄ both contribute to the separation and migration of
368 photogenerated electrons and holes. Moreover, the Ag@AgCl nanoislands on the porous g-
369 C₃N₄ nanosheets could provide many active centers by full exposing the adjacent area of
370 island-sheet interfaces to the pollutants. Similarly, porous N-TiO₂/g-C₃N₄ heterojunctions
371 prepared by Wang et al. degraded 100% RhB and MB within 40 and 60 min, respectively
372 with the *k* of 0.0284 and 0.07 min⁻¹ [93]. Other composites such as core-shell nanoplates N-
373 ZnO/g-C₃N₄, nanosheets MoS₂-TiO₂/g-C₃N₄ and so on all promoted the degradation efficacy
374 in some extent compared with the performance of the pristine and TiO₂ as shown in **Table 3**
375 [94-96]. Therefore, a conclusion can be drawn that compounding doping and morphology
376 controlling can effectively modified the g-C₃N₄ to possess higher photocatalytic ability for the
377 organic pollutants removal.

378

379 **4. Stability of g-C₃N₄ nanocomposites**

380 Besides the photocatalytic ability, the stability of the catalysts performing during the
381 photocatalysis procedure is also important for application on real water treatment. Thus, the

382 reusability and immobilization of the as-synthesized g-C₃N₄ nanocomposites are discussed in
383 the following section.

384 4.1. Reusability

385 In the practical photocatalytic applications in aqueous solution, the recycling of the
386 catalyst is essential task due to the leakage of the individual components during the
387 degradation process. Ag@AgCl-g-C₃N₄ porous nanosheets are taken as the representative
388 example because of comparatively high degradation efficacy and the reusability of this
389 catalyst is evaluated by recycling the photodegradation for RhB removal under visible light.
390 The results shown in **Fig. 3A** exhibit that only a slight decrease was observed after eight
391 consecutive photocatalysis, which proves that this materials have not only possess high
392 photocatalytic ability, but also excellent stability, which both contribute to a promising
393 visible-light driven catalyst on the application of pollutants removal. However, even though
394 the efficacy decrease during the recycling is minimum as shown in **Fig. 3A**, the small loss
395 will be enlarged with the change of catalysts content or the flow rate. Because no research on
396 g-C₃N₄ nanocomposites is conducted to this area, TiO₂ treatment is chose as the potential
397 evidence to be investigated. Li et al. used TiO₂ as catalyst for the continuous
398 photodegradation of dye wastewater and the COD removal rate was detected for the
399 evaluation of degradation efficacy [97]. **Fig. 3B** shows the Dye wastewater COD removed by
400 TiO₂ composites with different catalysts content and flow rates. The COD removal rate
401 increases with an increasing catalyst loading until 6.0 g L⁻¹ and subsequently decreases. Thus,
402 it is reasonable to predict that in the application of as-synthesized g-C₃N₄ nanocomposites, the
403 degradation efficacy of the pollutants removal will be decreased with the losing of catalysts
404 content during each cycle. Besides, the COD removal rate decreases with the increase of flow
405 rate, which is mainly caused by the decrease of photocatalytic time. So when the g-C₃N₄
406 composites deal with large volume of wastewater, the flow rate has an important effect on the
407 target pollutants removal and the efficacy will decreases quickly with the high flow rate.

408 Overall, the reusability of the as-synthesized catalysts should be further investigated as it is
409 reliant on many environmental factors.

410 4.2. Immobilization

411 The immobilization is an effectiveness method to promote the stability of catalysts by
412 providing a carrier according to the following methods: 1) the catalysts are evenly painted on
413 the smooth foundation to form a kind of continuous film; 2) the catalysts are doped with the
414 carrier to get the doping composites. Notably, the carrier should own the properties such as
415 well light transmission, strong binding force with the catalyst, strong adsorption of the
416 pollutants, large specific surface area and chemically inert. For example, Ye et al. fabricated
417 MoS₂/S-doped g-C₃N₄ heterojunction film to enhance photocatalytic degradation of MB with
418 visible light irradiation [98]. The CN film was prepared on the indium-tin oxide (ITO)
419 substrate and showed much stronger absorption with an abrupt gap of 430 nm. In another
420 instance, Dong et al. synthesized polymeric g-C₃N₄ doped on the structured Al₂O₃ ceramic
421 foam as a proper support for practical environmental application [99]. They found that Al₂O₃
422 ceramic foam were made up of connected arrays of struts and this design enabled the
423 immobilized g-C₃N₄ stable in activity and can be used repeatedly without deactivation. In
424 addition, the specific surface area of immobilized g-C₃N₄ was enlarged more than the pure g-
425 C₃N₄, which also make the Al₂O₃ ceramic foam an ideal carrier for immobilization of g-C₃N₄.
426 Therefore, the carrier could not only provide the immobilization of the catalyst, but also
427 promote the photocatalytic ability, which should be considered as a necessary decoration for
428 the g-C₃N₄ materials when they are applied in real wastewater.

429 Photocatalytic reactor is designed as the area of the photodegradation process for the
430 pollutants removal from water. As many reactors have been done for TiO₂ immobilization
431 while few are applied for g-C₃N₄, we redesigned these TiO₂ reactors to make them suitable
432 for the well immobilization and photodegradation performance of g-C₃N₄ nanocomposites
433 application. Basically, g-C₃N₄ catalysts only need visible light rather than UV light which is

434 necessary for TiO₂ due to the different adsorption ability of light source between the two
435 catalysts. Furthermore, pure g-C₃N₄ catalysts own the non-metal property so the leakage and
436 recycle of the metal should not be a problem to be considered. Normally the photocatalytic
437 experiments conducted in the laboratory use the suspension photocatalytic reactor as shown in
438 **Fig. 4A**. This kind of reactor possesses the advantages of simple structure, convenient
439 operation, non-limitation of compound transmission, and high rate of reaction. Nevertheless,
440 it also has several disadvantages; firstly, the particle size has strong influence on the
441 suspended state of the catalyst, namely, too small size would lead to a difficult separation
442 while too large would result in particles deposition. In addition, the particle size also affects
443 the light transmission as large size or high concentration would lead to the turbid solution so
444 that the light transmission will be disturbed and light adsorption is going to be reduced. More
445 important, the catalysts suspending in the solution is hard to be separated and re-used. Thus,
446 the loaded photocatalytic reactor is preferable to be used for the g-C₃N₄ nanocomposites
447 application. As shown in **Fig. 4B**, g-C₃N₄ on structured Al₂O₃ ceramic foam synthesized by
448 Dong et al. could be fixed at one side of the reaction pool and the pollutant water flows from
449 water intake to outlet passing through the loading g-C₃N₄ materials. However, such reactor
450 structure would easily present following two problems: one is the limited reaction area which
451 is just the cross-sectional area of the g-C₃N₄ on the Al₂O₃ foam; the other one is
452 comparatively short stay time of contacting the catalysts, which will lead to the incompletely
453 photodegradation. Accordingly, tubes, fibres, and floated glass balls have been designed for
454 the substitution of the single tiled catalysts. Notably, among them, fibres own the advantages
455 of large reaction area, low catalyst loss during the transmission, and high efficacy of optical
456 transmission. For instance, Hatat-Fraile et al. used the doped TiO₂ coated quartz fibre
457 membranes in a photocatalytic reactor as shown in **Fig. 4C** and it turned out to be durable
458 degradation ability with high efficacy [100]. In the same way, when g-C₃N₄ nanocomposites
459 take the place of TiO₂, it should achieve the similar degradation performance for the

460 pollutants removal. However, the fibre reactor also owns its drawbacks such as easy broken,
461 expensive, and difficult loading of the catalysts. Therefore, every kind of the photocatalytic
462 reactor should be taken into consideration when dealing with real wastewater.

463

464 5. Future perspectives

465 Although much research has been conducted about the g-C₃N₄ nanocatalysts, the
466 development application in photocatalysis is still at its early stage and there remain many
467 challenges.

468 5.1. Photocatalysis of POPs

469 As shown in the **Tables 1–3**, the main target compounds degraded by g-C₃N₄
470 composites are the dye pollutants such as the most common object of RhB, then MO, and
471 MB. Their molecular structures are provided in **Fig. S6A**. Based on the research of Wang et
472 al. [52], RhB could be degraded into CO₂ and H₂O by g-C₃N₄ nanocomposites under
473 simulated solar light irradiation. So it indicates that the photogenerated electron and hole pairs
474 in the photocatalytic system are able to broke the chemical bond including phenyl C-H bond,
475 C-O bond, and so on as shown in **Fig. S6A**. Notably, the bond dissociation energy (BDE) at
476 298 K of C-O bond reaches as high as 1077 kJ mol⁻¹ and then the BDE of phenyl C-H bond
477 could be 473 kJ mol⁻¹. Therefore, g-C₃N₄ can degrade other POPs existing in environmental
478 with visible light in theory. For example, as a classic kind of perfluoroalkyl
479 substances(PFAS), perfluorooctanoic acid (PFOA) recently draw a great attention as they are
480 potential reproductive and developmental toxins, endocrine disrupters, and carcinogens [101].
481 More serious, PFOA was detected in high concentration in the environmental media and hard
482 to be degraded due to the strong C-F bond (BDE is 544 kJ mol⁻¹) as shown in the structure
483 (**Fig. S6B**). Li et al. used the commercial In₂O₃ nanocrystals and the results showed that they
484 could degraded 80% PFOA within 180 min under UV irradiation [102]. Besides, Chen et al.
485 successfully synthesized In₂O₃/g-C₃N₄ composites and the as-synthesized catalysts was

486 proved to be able to degrade almost RhB under visible light irradiation [103]. Thus, it is
487 reasonable to provide a suspicion that $\text{In}_2\text{O}_3/\text{g-C}_3\text{N}_4$ composites can degrade PFOA more
488 efficiently than commercial In_2O_3 or pure $\text{g-C}_3\text{N}_4$. The reason may be attributed to that the
489 doping composites should have a better band gap and the recombination of photogenerated
490 electron and hole pairs should be inhibited as the function of composite structure. more details
491 about the specific degradation and simulation process are available in **Eqs. (S1)–(S12)** (See
492 appendix...). Therefore, PFOA photodegraded by $\text{In}_2\text{O}_3/\text{g-C}_3\text{N}_4$ catalysts are worthwhile to be
493 investigated in the future because it could prove a novel materials able to deal with the PFAS
494 efficiently.

495 5.2. Influence of environmental conditions

496 Many environmental conditions during the photodegradation process such as solution
497 pH, reaction temperature, DO, and dissolved organic matters (DOM) play the significant
498 factors for the photocatalytic performance while these factors were seldom investigated in the
499 previous research of $\text{g-C}_3\text{N}_4$ photocatalysis. The solution pH would influence the ionization
500 degree of the chemical compounds and largely decide their positive or negative charged. The
501 opposite charged of the pollutants and the catalysts could promote the combination between
502 them and thus increase the photodegradation efficacy. In addition, the reaction temperature
503 would lead to a high impact for the photodegradation progress. Because high temperature is
504 able to accelerate the redox reaction, however, too high temperature would change the
505 nanostructure of the catalyst which leads to the catalyst deactivation. Besides, DO plays an
506 important role in degrading the pollutants. As shown in Eq. 2, the oxygen in the solution
507 could react with electron to produce the $\bullet\text{O}_2^-$, which has the oxidation ability to deal with the
508 pollutants as the same function of photogenerated h^+ and in the meantime it can inhibit the
509 recombination of electron and hole pairs due to the consumption of electron. Furthermore,
510 DOM normally exists in the real water and considered to have a pronounced effect on
511 photochemical because of the generation of DOM-derived oxidative intermediates or their

512 physicochemical quenching effects. On one hand, DOM will occupy the surface of the
513 catalysts instead of the target pollutant, which lead to the less adsorption capacity of the
514 catalysts and poor degradation efficacy. Furthermore, DOM such as humic acid in the
515 reaction mixture absorb the photon and generated active groups such as $\bullet\text{OH}$ or $\bullet\text{O}_2^-$ and thus
516 would affect the photooxidation rate [104]. These environmental conditions have been proven
517 to have significant effect on the catalytic ability of TiO_2 in the previous literatures [104-107].
518 Therefore, when a new kind of g- C_3N_4 composites is synthesized, pH, reaction temperature,
519 DO, and DOM should be investigated to determinate the best conditions for the photocatalytic
520 performance of the as-synthesized catalysts.

521 Some other significant points in the future research are including as follows:

- 522 ❖ Synthesizing innovative g- C_3N_4 composites which are benefit in the morphology
523 controlling or the new compound doping;
- 524 ❖ Investigating the application on the real wastewater and evaluating the
525 photocatalytic ability of different g- C_3N_4 composites, combining with their cost
526 in commercial and energy consuming;
- 527 ❖ Designing the suitable material as the carrier to promote the immobilization of g-
528 C_3N_4 composites which can inhibit the catalyst loss during degradation process;
- 529 ❖ Investigating other significant persistent organic pollutants (POPs) such as
530 Polybrominated diphenyl ethers (PBDEs) [108, 109], Hexabromocyclododecane
531 (HBCDs) [110], Endocrine disrupting chemicals (EDCs) [111], pharmaceuticals
532 [112], etc. conducted by g- C_3N_4 composites under visible light irradiation and
533 evaluating their photodegradation efficacy.

534

535 6. Conclusions

536 In summary, g- C_3N_4 possesses higher photocatalytic ability than TiO_2 for some
537 organic pollutants, which is probably attributed to the suitable band gap energy and good

538 redox ability of the photogenerated carriers. However, owing to the drawbacks of low surface
539 are and fast recombination of photogenerated electron and hole pairs, element and
540 compounding doping are summarized and their degradation efficacy have been compared. As
541 a conclusion, among metal doping, K doping promoted most degrading efficacy with the k
542 value of 0.0110 min^{-1} than other metal performance. And C, as a present of non-metal doping,
543 promoted 3.0 times of rate constant for RhB degradation than origin g-C₃N₄. In addition,
544 when two semiconductors with different CB and VB potentials are doped together as
545 heterojunction, the photogenerated electrons and holes could transfer from the energy level of
546 one semiconductor to another's and thus inhibits the recombination of electron and hole pairs
547 in single material. Notably, Z-Scheme composite doping, such as Z-Scheme Ag₃PO₄-g-C₃N₄,
548 have outstanding degradation efficacy, which could degrade 100% MO within 5 min with k of
549 0.2357 min^{-1} under visible light irradiation. Besides, morphology controlling and co-doping
550 can further promoted the catalytic ability. For example, Ag@AgCl-g-C₃N₄ porous nanosheets
551 degraded degrade RhB, MB, MO, and Phenol all with high k value of 0.1954, 0.0258, 0.0260,
552 0.0128 min^{-1} , respectively. Besides, those reported g-C₃N₄ composites all have well
553 reusability according to the repeated photocatalysis experiments. However, when the catalyst
554 dose or the flow rate of the solution increases, the photodegradation rate would be negatively
555 influenced. Notably, the immobilization is the significant method to promote the stability of
556 the catalyst in application, which mainly includes carriers fabricating and photo reactor
557 designing. And future work should be focus on the other meaningful POPs photodegradation
558 by these as-synthesized g-C₃N₄ composites and environmental conditions discussion during
559 the photocatalysis process. In the meantime, we still have to devote to synthesize more
560 functionalized yet low-cost g-C₃N₄ composites to decompose the environmental organic
561 pollutant with high and stable efficacy.

562

563 **Acknowledgements**

564 The authors would like to thank the China Scholarship Council (CSC) for the financial
565 support (Grant No. 201606890028).

567 **References**

- 568 1. Bahnemann, D., *Photocatalytic water treatment: solar energy applications*. Solar energy, 2004. **77**(5): p. 445-459.
- 569 2. Malato, S., et al., *Photocatalysis with solar energy at a pilot-plant scale: an overview*. Applied Catalysis B: Environmental, 2002. **37**(1): p. 1-15.
- 570 3. Stilwell, D.E. and S.M. Park, *Electrochemistry of conductive polymers IV electrochemical studies on polyaniline degradation—Product identification and coulometric studies*. Journal of the Electrochemical Society, 1988. **135**(10): p. 2497-2502.
- 571 4. Simon, A., et al., *Effects of membrane degradation on the removal of pharmaceutically active compounds (PhACs) by NF/RO filtration processes*. Journal of Membrane Science, 2009. **340**(1): p. 16-25.
- 572 5. Pagga, U. and D. Brown, *The degradation of dyestuffs: Part II Behaviour of dyestuffs in aerobic biodegradation tests*. Chemosphere, 1986. **15**(4): p. 479-491.
- 573 6. Quintana, J.B., S. Weiss, and T. Reemtsma, *Pathways and metabolites of microbial degradation of selected acidic pharmaceutical and their occurrence in municipal wastewater treated by a membrane bioreactor*. Water research, 2005. **39**(12): p. 2654-2664.
- 574 7. Xu, B., et al., *Photocatalytic removal of perfluoroalkyl substances from water and wastewater: Mechanism, kinetics and controlling factors*. Chemosphere, 2017.
- 575 8. He, F., *Review in the TiO₂ Photocatalytic Degradation of Organic Matter in Radioactive Waste Water*. DEStech Transactions on Environment, Energy and Earth Science, 2017(apeesd).
- 576 9. Konyar, M., et al., *Reticulated ZnO Photocatalyst: Efficiency Enhancement in Degradation of Acid Red 88 Azo Dye by Catalyst Surface Cleaning*. Chemical Engineering Communications, 2017. **204**(6): p. 705-710.
- 577 10. He, H.-Y., *Facile synthesis of Bi₂S₃ nanocrystalline-modified TiO₂: Fe nanotubes hybrids and their photocatalytic activities in dye degradation*. Particulate Science and Technology, 2017. **35**(4): p. 410-417.
- 578 11. Zhou, L., et al., *A novel ternary visible-light-driven photocatalyst AgCl/Ag₃PO₄/g-C₃N₄: Synthesis, characterization, photocatalytic activity for antibiotic degradation and mechanism analysis*. Catalysis Communications, 2017. **100**: p. 191-195.
- 579 12. Sornalingam, K., et al., *Photocatalysis of estrone in water and wastewater: Comparison between Au-TiO₂ nanocomposite and TiO₂, and degradation by-products*. Science of The Total Environment, 2018. **610**: p. 521-530.
- 580 13. Zhao, Z., Y. Sun, and F. Dong, *Graphitic carbon nitride based nanocomposites: a review*. Nanoscale, 2015. **7**(1): p. 15-37.
- 581 14. Teter, D.M. and R.J. Hemley, *Low-compressibility carbon nitrides*. Science, 1996. **271**(5245): p. 53.
- 582 15. Zhu, B., et al., *First principle investigation of halogen-doped monolayer gC₃N₄ photocatalyst*. Applied Catalysis B: Environmental, 2017. **207**: p. 27-34.
- 583 16. Shi, L., et al., *In site acid template induced facile synthesis of porous graphitic carbon nitride with enhanced visible-light photocatalytic activity*. Catalysis Communications, 2017. **89**: p. 129-132.
- 584 17. Wen, J., et al., *A review on gC₃N₄-based photocatalysts*. Applied Surface Science, 2017. **391**: p. 72-123.
- 585 18. Chen, X., Y. Dai, and X. Wang, *Methods and mechanism for improvement of photocatalytic activity and stability of Ag₃PO₄: A review*. Journal of Alloys and Compounds, 2015. **649**: p. 910-932.
- 586 19. Patnaik, S., et al., *An overview of the modification of g-C₃N₄ with high carbon containing materials for photocatalytic applications*. Inorg. Chem. Front., 2016. **3**(3): p. 336-347.
- 587
- 588
- 589
- 590
- 591
- 592
- 593
- 594
- 595
- 596
- 597
- 598
- 599
- 600
- 601
- 602
- 603
- 604
- 605
- 606
- 607
- 608
- 609
- 610
- 611
- 612
- 613
- 614
- 615

- 616 20. Cao, S., et al., *Polymeric photocatalysts based on graphitic carbon nitride*. *Advanced*
617 *Materials*, 2015. **27**(13): p. 2150-2176.
- 618 21. Mamba, G. and A. Mishra, *Graphitic carbon nitride (gC₃N₄) nanocomposites: A new and*
619 *exciting generation of visible light driven photocatalysts for environmental pollution*
620 *remediation*. *Applied Catalysis B: Environmental*, 2016. **198**: p. 347-377.
- 621 22. Niu, P., et al., *Graphene-like carbon nitride nanosheets for improved photocatalytic activities*.
622 *Advanced Functional Materials*, 2012. **22**(22): p. 4763-4770.
- 623 23. Liao, G., et al., *Graphene oxide modified gC₃N₄ hybrid with enhanced photocatalytic*
624 *capability under visible light irradiation*. *Journal of Materials Chemistry*, 2012. **22**(6): p. 2721-
625 2726.
- 626 24. Yan, S., Z. Li, and Z. Zou, *Photodegradation performance of g-C₃N₄ fabricated by directly*
627 *heating melamine*. *Langmuir*, 2009. **25**(17): p. 10397-10401.
- 628 25. Wang, S., et al., *Synthesis and characterization of gC₃N₄/Ag₃VO₄ composites with*
629 *significantly enhanced visible-light photocatalytic activity for triphenylmethane dye*
630 *degradation*. *Applied Catalysis B: Environmental*, 2014. **144**: p. 885-892.
- 631 26. Liu, J., et al., *Simple pyrolysis of urea into graphitic carbon nitride with recyclable adsorption*
632 *and photocatalytic activity*. *Journal of Materials Chemistry*, 2011. **21**(38): p. 14398-14401.
- 633 27. Wu, T., et al., *Photoassisted degradation of dye pollutants. V. Self-photosensitized oxidative*
634 *transformation of rhodamine B under visible light irradiation in aqueous TiO₂ dispersions*. *The*
635 *Journal of Physical Chemistry B*, 1998. **102**(30): p. 5845-5851.
- 636 28. Ren, H.-T., et al., *Improved photochemical reactivities of Ag₂O/g-C₃N₄ in phenol degradation*
637 *under UV and visible light*. *Industrial & Engineering Chemistry Research*, 2014. **53**(45): p.
638 17645-17653.
- 639 29. Jo, W.-K., et al., *Synthesis of MoS₂ nanosheet supported Z-scheme TiO₂/gC₃N₄*
640 *photocatalysts for the enhanced photocatalytic degradation of organic water pollutants*. *RSC*
641 *Advances*, 2016. **6**(13): p. 10487-10497.
- 642 30. Ma, S., et al., *Enhanced disinfection application of Ag-modified gC₃N₄ composite under*
643 *visible light*. *Applied Catalysis B: Environmental*, 2016. **186**: p. 77-87.
- 644 31. Li, Z., C. Kong, and G. Lu, *Visible photocatalytic water splitting and photocatalytic two-*
645 *electron oxygen formation over Cu- and Fe-doped g-C₃N₄*. *The Journal of Physical Chemistry*
646 *C*, 2015. **120**(1): p. 56-63.
- 647 32. Wang, X., et al., *A metal-free polymeric photocatalyst for hydrogen production from water*
648 *under visible light*. *Nature materials*, 2009. **8**(1): p. 76-80.
- 649 33. Shi, H., et al., *Polymeric g-C₃N₄ coupled with NaNbO₃ nanowires toward enhanced*
650 *photocatalytic reduction of CO₂ into renewable fuel*. *Acs Catalysis*, 2014. **4**(10): p. 3637-3643.
- 651 34. Cao, S. and J. Yu, *g-C₃N₄-based photocatalysts for hydrogen generation*. *The journal of*
652 *physical chemistry letters*, 2014. **5**(12): p. 2101-2107.
- 653 35. Jiang, L., et al., *Doping of graphitic carbon nitride for photocatalysis: A review*. *Applied*
654 *Catalysis B: Environmental*, 2017. **217**: p. 388-406.
- 655 36. Liang, Q., et al., *Hydrothermal fabrication of α-SnWO₄/g-C₃N₄ heterostructure with*
656 *enhanced visible-light photocatalytic activity*. *Journal of Materials Science: Materials in*
657 *Electronics*, 2017: p. 1-5.
- 658 37. Jiang, Y., et al., *Construction of amorphous Ta₂O₅/gC₃N₄ nanosheet hybrids with superior*
659 *visible-light photoactivities for organic dye degradation and mechanism insight*. *Separation*
660 *and Purification Technology*, 2016. **170**: p. 10-21.
- 661 38. Xu, B., et al., *Photocatalytic removal of perfluoroalkyl substances from water and*
662 *wastewater: Mechanism, kinetics and controlling factors*. *Chemosphere*, 2017. **189**: p. 717-
663 729.
- 664 39. Liu, L., et al., *Organic Semiconductor g-C₃N₄Modified TiO₂Nanotube Arrays for Enhanced*
665 *Photoelectrochemical Performance in Wastewater Treatment*. *Energy Technology*, 2015. **3**(9):
666 p. 982-988.

- 667 40. Song, G., et al., *Enhanced performance of g-C₃N₄/TiO₂ photocatalysts for degradation of*
668 *organic pollutants under visible light*. Chinese Journal of Chemical Engineering, 2015. **23**(8):
669 p. 1326-1334.
- 670 41. Tang, H., et al., *Novel spindle-shaped nanoporous TiO₂ coupled graphitic g-C₃N₄ nanosheets*
671 *with enhanced visible-light photocatalytic activity*. Ceramics International, 2016. **42**(16): p.
672 18443-18452.
- 673 42. Song, X., et al., *Synthesis of Fe/g-C₃N₄ composites with improved visible light photocatalytic*
674 *activity*. Materials Letters, 2014. **116**: p. 265-267.
- 675 43. Le, S., et al., *Cu-doped mesoporous graphitic carbon nitride for enhanced visible-light driven*
676 *photocatalysis*. RSC Adv., 2016. **6**(45): p. 38811-38819.
- 677 44. Chen, S., et al., *Fabrication and characterization of novel Z-scheme photocatalyst WO₃/g-*
678 *C₃N₄ with high efficient visible light photocatalytic activity*. Materials Chemistry and Physics,
679 2015. **149-150**: p. 512-521.
- 680 45. Tian, Y., et al., *Hydrothermal synthesis of graphitic carbon nitride-Bi₂WO₆ heterojunctions*
681 *with enhanced visible light photocatalytic activities*. ACS Appl Mater Interfaces, 2013. **5**(15):
682 p. 7079-85.
- 683 46. Xu, D., et al., *Synthesis and photocatalytic performance of europium-doped graphitic carbon*
684 *nitride*. Journal of Rare Earths, 2013. **31**(11): p. 1085-1091.
- 685 47. Xiong, T., et al., *Bridging the g-C₃N₄ interlayers for enhanced photocatalysis*. ACS Catalysis,
686 2016. **6**(4): p. 2462-2472.
- 687 48. Zheng, Y., et al., *Graphitic carbon nitride polymers toward sustainable photoredox catalysis*.
688 *Angewandte Chemie International Edition*, 2015. **54**(44): p. 12868-12884.
- 689 49. Zhang, J., S. Hu, and Y. Wang, *A convenient method to prepare a novel alkali metal sodium*
690 *doped carbon nitride photocatalyst with a tunable band structure*. RSC Adv., 2014. **4**(108): p.
691 62912-62919.
- 692 50. Jin, R., et al., *A Convenient Method to Prepare Novel Rare Earth Metal Ce-Doped Carbon*
693 *Nitride with Enhanced Photocatalytic Activity Under Visible Light*. Bulletin of the Korean
694 Chemical Society, 2015. **36**(1): p. 17-23.
- 695 51. Wang, Y., et al., *Facile synthesis of Y-doped graphitic carbon nitride with enhanced*
696 *photocatalytic performance*. Catalysis Communications, 2016. **84**: p. 179-182.
- 697 52. Wang, Y., et al., *Simple synthesis of Zr-doped graphitic carbon nitride towards enhanced*
698 *photocatalytic performance under simulated solar light irradiation*. Catalysis
699 *Communications*, 2015. **72**: p. 24-28.
- 700 53. Rong, X., et al., *Enhanced visible light photocatalytic activity of W-doped porous g-C₃N₄ and*
701 *effect of H₂O₂*. Materials Letters, 2016. **164**: p. 127-131.
- 702 54. Hu, S., et al., *Band gap-tunable potassium doped graphitic carbon nitride with enhanced*
703 *mineralization ability*. Dalton Trans, 2015. **44**(3): p. 1084-92.
- 704 55. Dong, G., et al., *A fantastic graphitic carbon nitride (gC₃N₄) material: electronic structure,*
705 *photocatalytic and photoelectronic properties*. Journal of Photochemistry and Photobiology
706 C: Photochemistry Reviews, 2014. **20**: p. 33-50.
- 707 56. Fan, Q., et al., *A simple fabrication for sulfur doped graphitic carbon nitride porous rods with*
708 *excellent photocatalytic activity degrading RhB dye*. Applied Surface Science, 2017. **391**: p.
709 360-368.
- 710 57. Yan, S.C., Z.S. Li, and Z.G. Zou, *Photodegradation of rhodamine B and methyl orange over*
711 *boron-doped g-C₃N₄ under visible light irradiation*. Langmuir, 2010. **26**(6): p. 3894-901.
- 712 58. RUAN, L.-W., et al., *Analysis of Electrical and Optical Properties of g-C₃N₄ with Carbon-*
713 *Position Doping*. Acta Physico-Chimica Sinica, 2014. **30**(1): p. 43-52.
- 714 59. Zuo, F., et al., *Self-doped Ti³⁺ enhanced photocatalyst for hydrogen production under visible*
715 *light*. Journal of the American Chemical Society, 2010. **132**(34): p. 11856-11857.
- 716 60. Zhang, X. and L. Zhang, *Electronic and band structure tuning of ternary semiconductor*
717 *photocatalysts by self doping: the case of BiOI*. The Journal of Physical Chemistry C, 2010.
718 **114**(42): p. 18198-18206.

- 719 61. Xie, K., et al., *Self-doped SrTiO₃- δ photocatalyst with enhanced activity for artificial*
720 *photosynthesis under visible light*. Energy & Environmental Science, 2011. **4**(10): p. 4211-
721 4219.
- 722 62. Dong, G., K. Zhao, and L. Zhang, *Carbon self-doping induced high electronic conductivity and*
723 *photoreactivity of g-C₃N₄*. Chem Commun (Camb), 2012. **48**(49): p. 6178-80.
- 724 63. Zhang, Y., et al., *Porous graphitic carbon nitride synthesized via direct polymerization of urea*
725 *for efficient sunlight-driven photocatalytic hydrogen production*. Nanoscale, 2012. **4**(17): p.
726 5300-5303.
- 727 64. Zhang, M., et al., *Enhanced catalytic activity of potassium-doped graphitic carbon nitride*
728 *induced by lower valence position*. Applied Catalysis B: Environmental, 2015. **164**: p. 77-81.
- 729 65. Tonda, S., et al., *Fe-doped and -mediated graphitic carbon nitride nanosheets for enhanced*
730 *photocatalytic performance under natural sunlight*. Journal of Materials Chemistry A, 2014.
731 **2**(19): p. 6772.
- 732 66. Hu, S., et al., *A simple and efficient method to prepare a phosphorus modified g-C₃N₄ visible*
733 *light photocatalyst*. RSC Adv., 2014. **4**(41): p. 21657-21663.
- 734 67. Chai, B., et al., *Enhanced visible light photocatalytic degradation of Rhodamine B over*
735 *phosphorus doped graphitic carbon nitride*. Applied Surface Science, 2017. **391**: p. 376-383.
- 736 68. Zhang, L., et al., *Facile synthesis of phosphorus doped graphitic carbon nitride polymers with*
737 *enhanced visible-light photocatalytic activity*. Materials Research Bulletin, 2013. **48**(9): p.
738 3485-3491.
- 739 69. Zhu, H., et al., *In-situ synthesis of g-C₃N₄-P₂₅ TiO₂ composite with enhanced visible light*
740 *photoactivity*. Journal of Nanoparticle Research, 2014. **16**(10).
- 741 70. Wang, W., et al., *Synthesis of Hierarchical TiO₂-C₃N₄ Hybrid Microspheres with Enhanced*
742 *Photocatalytic and Photovoltaic Activities by Maximizing the Synergistic Effect*.
743 ChemPhotoChem, 2017. **1**(1): p. 35-45.
- 744 71. Xu, M., L. Han, and S. Dong, *Facile fabrication of highly efficient g-C₃N₄/Ag₂O*
745 *heterostructured photocatalysts with enhanced visible-light photocatalytic activity*. ACS Appl
746 Mater Interfaces, 2013. **5**(23): p. 12533-40.
- 747 72. Jiang, D., et al., *Two-Dimensional CaIn₂S₄/g-C₃N₄ Heterojunction Nanocomposite with*
748 *Enhanced Visible-Light Photocatalytic Activities: Interfacial Engineering and Mechanism*
749 *Insight*. ACS Appl Mater Interfaces, 2015. **7**(34): p. 19234-42.
- 750 73. Ke, Y., et al., *ZrO₂/g-C₃N₄ with enhanced photocatalytic degradation of methylene blue*
751 *under visible light irradiation*. Journal of Materials Research, 2014. **29**(20): p. 2473-2482.
- 752 74. Lv, J., et al., *Facile synthesis of Z-scheme graphitic-C₃N₄/Bi₂MoO₆ nanocomposite for*
753 *enhanced visible photocatalytic properties*. Applied Surface Science, 2015. **358**: p. 377-384.
- 754 75. Zhang, J., et al., *Design of a direct Z-scheme photocatalyst: preparation and characterization*
755 *of Bi₂O₃/g-C₃N₄ with high visible light activity*. J Hazard Mater, 2014. **280**: p. 713-22.
- 756 76. Liu, Y., et al., *Enhanced visible-light photocatalytic activity of Z-scheme graphitic carbon*
757 *nitride/oxygen vacancy-rich zinc oxide hybrid photocatalysts*. Chinese Journal of Catalysis,
758 2015. **36**(12): p. 2135-2144.
- 759 77. Fu, J., et al., *Novel C₃N₄-CdS composite photocatalysts with organic-inorganic*
760 *heterojunctions: in situ synthesis, exceptional activity, high stability and photocatalytic*
761 *mechanism*. Journal of Materials Chemistry A, 2013. **1**(9): p. 3083.
- 762 78. Fu, J., et al., *BiOBr-carbon nitride heterojunctions: synthesis, enhanced activity and*
763 *photocatalytic mechanism*. Journal of Materials Chemistry, 2012. **22**(39): p. 21159.
- 764 79. Katsumata, H., et al., *Highly Efficient Photocatalytic Activity of g-C₃N₄/Ag₃PO₄ Hybrid*
765 *Photocatalysts through Z-Scheme Photocatalytic Mechanism under Visible Light*. Industrial &
766 Engineering Chemistry Research, 2014. **53**(19): p. 8018-8025.
- 767 80. Ma, D., et al., *Fabrication of Z-scheme g-C₃N₄/RGO/Bi₂WO₆ photocatalyst with*
768 *enhanced visible-light photocatalytic activity*. Chemical Engineering Journal, 2016. **290**: p.
769 136-146.

- 770 81. Hong, Y., et al., *In-situ synthesis of direct solid-state Z-scheme V₂O₅/g-C₃N₄*
771 *heterojunctions with enhanced visible light efficiency in photocatalytic degradation of*
772 *pollutants*. Applied Catalysis B: Environmental, 2016. **180**: p. 663-673.
- 773 82. He, Y., et al., *Z-scheme SnO₂-x/g-C₃N₄ composite as an efficient photocatalyst for dye*
774 *degradation and photocatalytic CO₂ reduction*. Solar Energy Materials and Solar Cells, 2015.
775 **137**: p. 175-184.
- 776 83. He, Y., et al., *Synthesis, Characterization, and Activity Evaluation of DyVO₄/g-*
777 *C₃N₄Composites under Visible-Light Irradiation*. Industrial & Engineering Chemistry Research,
778 2012. **51**(45): p. 14729-14737.
- 779 84. He, Y., et al., *Efficient degradation of RhB over GdVO₄/g-C₃N₄ composites under visible-light*
780 *irradiation*. Chemical Engineering Journal, 2013. **215-216**: p. 721-730.
- 781 85. Adhikari, S.P., et al., *Electrospinning Directly Synthesized Porous TiO₂ Nanofibers Modified by*
782 *Graphitic Carbon Nitride Sheets for Enhanced Photocatalytic Degradation Activity under Solar*
783 *Light Irradiation*. Langmuir, 2016. **32**(24): p. 6163-75.
- 784 86. Li, F.-t., et al., *Precipitation Synthesis of Mesoporous Photoactive Al₂O₃for Constructing g-*
785 *C₃N₄-Based Heterojunctions with Enhanced Photocatalytic Activity*. Industrial & Engineering
786 Chemistry Research, 2014: p. 141205091652003.
- 787 87. Chen, X., et al., *Growth of gC₃N₄ on mesoporous TiO₂ spheres with high photocatalytic*
788 *activity under visible light irradiation*. Applied Catalysis B: Environmental, 2016. **188**: p. 342-
789 350.
- 790 88. Wu, Y., et al., *TiO₂/g-C₃N₄ nanosheets hybrid photocatalyst with enhanced photocatalytic*
791 *activity under visible light irradiation*. Research on Chemical Intermediates, 2015. **42**(4): p.
792 3609-3624.
- 793 89. Dong, Y., et al., *Morphological control of tubular g-C₃N₄ and their visible-light*
794 *photocatalytic properties*. Materials Letters, 2017. **196**: p. 100-103.
- 795 90. Chen, Y., et al., *Construction of heterostructured g-C(3)N(4)/Ag/TiO(2) microspheres with*
796 *enhanced photocatalysis performance under visible-light irradiation*. ACS Appl Mater
797 Interfaces, 2014. **6**(16): p. 14405-14.
- 798 91. Dai, K., et al., *Heterojunction of facet coupled g-C₃N₄/surface-fluorinated TiO₂ nanosheets*
799 *for organic pollutants degradation under visible LED light irradiation*. Applied Catalysis B:
800 Environmental, 2014. **156-157**: p. 331-340.
- 801 92. Zhang, S., et al., *In situ ion exchange synthesis of strongly coupled Ag@AgCl/g-C(3)N(4)*
802 *porous nanosheets as plasmonic photocatalyst for highly efficient visible-light photocatalysis*.
803 ACS Appl Mater Interfaces, 2014. **6**(24): p. 22116-25.
- 804 93. Wang, X.-j., et al., *In Situ Microwave-Assisted Synthesis of Porous N-TiO₂/g-*
805 *C₃N₄Heterojunctions with Enhanced Visible-Light Photocatalytic Properties*. Industrial &
806 Engineering Chemistry Research, 2013. **52**(48): p. 17140-17150.
- 807 94. Kumar, S., et al., *Cost-effective and eco-friendly synthesis of novel and stable N-doped ZnO/g-*
808 *C₃N₄ core-shell nanoplates with excellent visible-light responsive photocatalysis*. Nanoscale,
809 2014. **6**(9): p. 4830-42.
- 810 95. Jo, W.-K., et al., *Synthesis of MoS₂nanosheet supported Z-scheme TiO₂/g-*
811 *C₃N₄photocatalysts for the enhanced photocatalytic degradation of organic water*
812 *pollutants*. RSC Adv., 2016. **6**(13): p. 10487-10497.
- 813 96. Li, K., et al., *Synergetic Effect of Ti³⁺ and Oxygen Doping on Enhancing Photoelectrochemical*
814 *and Photocatalytic Properties of TiO₂/g-C₃N₄ Heterojunctions*. ACS Appl Mater Interfaces,
815 2017. **9**(13): p. 11577-11586.
- 816 97. Li, Y., et al., *Activated carbon supported TiO₂-photocatalysis doped with Fe ions fo continuous*
817 *treatment of dye wastewater in a dynamic reactor*. Journal of Environmental Sciences, 2010.
818 **22**(8): p. 1290-1296.
- 819 98. Ye, L., D. Wang, and S. Chen, *Fabrication and Enhanced Photoelectrochemical Performance of*
820 *MoS(2)/S-Doped g-C(3)N(4) Heterojunction Film*. ACS Appl Mater Interfaces, 2016. **8**(8): p.
821 5280-9.

- 822 99. Dong, F., et al., *Immobilization of polymeric g-C₃N₄ on structured ceramic foam for efficient*
823 *visible light photocatalytic air purification with real indoor illumination.* Environ Sci Technol,
824 2014. **48**(17): p. 10345-53.
- 825 100. Hatat-Fraile, M., et al., *Concurrent photocatalytic and filtration processes using doped TiO₂*
826 *coated quartz fiber membranes in a photocatalytic membrane reactor.* Chemical Engineering
827 Journal, 2017. **330**: p. 531-540.
- 828 101. Goulding, D.R., et al., *Gestational exposure to perfluorooctanoic acid (PFOA): Alterations in*
829 *motor related behaviors.* Neurotoxicology, 2017. **58**: p. 110-119.
- 830 102. Li, Z., et al., *In₂O₃ nanoporous nanosphere: A highly efficient photocatalyst for decomposition*
831 *of perfluorooctanoic acid.* Applied Catalysis B: Environmental, 2012. **125**: p. 350-357.
- 832 103. Chen, L.-Y. and W.-D. Zhang, *In₂O₃/g-C₃N₄ composite photocatalysts with enhanced visible*
833 *light driven activity.* Applied Surface Science, 2014. **301**: p. 428-435.
- 834 104. Lyu, X.-J., et al., *Photodegradation of perfluorooctane sulfonate in environmental matrices.*
835 *Separation and Purification Technology*, 2015. **151**: p. 172-176.
- 836 105. Giri, R.R., et al., *Factors influencing UV photodecomposition of perfluorooctanoic acid in*
837 *water.* Chemical Engineering Journal, 2012. **180**: p. 197-203.
- 838 106. Lee, Y.C., et al., *Microwave-hydrothermal decomposition of perfluorooctanoic acid in water*
839 *by iron-activated persulfate oxidation.* Water Res, 2010. **44**(3): p. 886-92.
- 840 107. Zhao, B., et al., *ss-Ga₂O₃ nanorod synthesis with a one-step microwave irradiation*
841 *hydrothermal method and its efficient photocatalytic degradation for perfluorooctanoic acid.*
842 *Photochem Photobiol*, 2015. **91**(1): p. 42-7.
- 843 108. Wu, M.H., et al., *Occurrence and profiles of polybrominated diphenyl ethers (PBDEs) in*
844 *riverine sediments of Shanghai: a combinative study with human serum from the locals.*
845 *Environ Geochem Health*, 2017. **39**(4): p. 729-738.
- 846 109. Xu, B., et al., *Aquatic photolysis of hydroxylated polybromodiphenyl ethers under direct UV*
847 *irradiation: a case study of 2'-HO-BDE-68.* Environ Sci Pollut Res Int, 2017. **24**(16): p. 14409-
848 14416.
- 849 110. Wu, M.H., et al., *Occurrence of Hexabromocyclododecane in soil and road dust from mixed-*
850 *land-use areas of Shanghai, China, and its implications for human exposure.* Sci Total Environ,
851 2016. **559**: p. 282-90.
- 852 111. Wu, M., et al., *Chemical analysis of fish bile extracts for monitoring endocrine disrupting*
853 *chemical exposure in water: Bisphenol A, alkylphenols, and norethindrone.* Environ Toxicol
854 Chem, 2016. **35**(1): p. 182-90.
- 855 112. Archer, E., et al., *The fate of pharmaceuticals and personal care products (PPCPs), endocrine*
856 *disrupting contaminants (EDCs), metabolites and illicit drugs in a WWTW and environmental*
857 *waters.* Chemosphere, 2017. **174**: p. 437-446.

858